

MoLAN: A Unified Modality-Aware Noise Dynamic Editing Framework for Multimodal Sentiment Analysis

Xingle Xu, Yongkang Liu, Dexian Cai, Shi Feng*, Xiaocui Yang, Daling Wang, Yifei Zhang

Northeastern University, China

xuxingle@stumail.neu.edu.cn, 2301840@stu.neu.edu.cn, misonsky@163.com, fengshi, yangxiaocui, wangdaling, zhangyifei}@cse.neu.edu.cn

Abstract

Multimodal Sentiment Analysis aims to integrate information from various modalities, such as audio, visual, and text, to make complementary predictions. However, it often struggles with irrelevant or misleading visual and auditory information. Most existing approaches typically treat the entire modality information (e.g., a whole image, audio segment, or text paragraph) as an independent unit for feature enhancement or denoising. They often suppress the redundant and noise information at the risk of losing critical information. To address this challenge, we propose **MoLAN**, a unified **ModaLity**-aware noise dynAmic editiNg framework. Specifically, MoLAN performs modality-aware blocking by dividing the features of each modality into multiple blocks. Each block is then dynamically assigned a distinct denoising strength based on its noise level and semantic relevance, enabling fine-grained noise suppression while preserving essential multimodal information. Notably, MoLAN is a unified and flexible framework that can be seamlessly integrated into a wide range of multimodal models. Building upon this framework, we further introduce **MoLAN⁺**, a new multimodal sentiment analysis approach. Experiments across five models and four datasets demonstrate the broad effectiveness of the MoLAN framework. Extensive evaluations show that MoLAN⁺ achieves the state-of-the-art performance. The code is publicly available at <https://github.com/betterfly123/MoLAN-Framework>.

Introduction

The development demands of Artificial General Intelligence increase attention toward Multimodal Sentiment Analysis (MSA). MSA aims to integrate information from various modalities, such as text, visual, and audio data, to achieve a more comprehensive and accurate understanding of the emotions expressed by users or the environment (Zadeh et al. 2018b; Morency, Mihalcea, and Doshi 2011). MSA holds significant academic value in advancing multimodal learning and cross-modal understanding, and offers broad industrial applications in areas such as human-computer interaction and mental health monitoring (Das and Singh 2023; Pantic and Rothkrantz 2003; Zhou et al. 2015).

Most existing methods for MSA achieve impressive improvements by leveraging the synergistic effects of multiple

*Corresponding author.

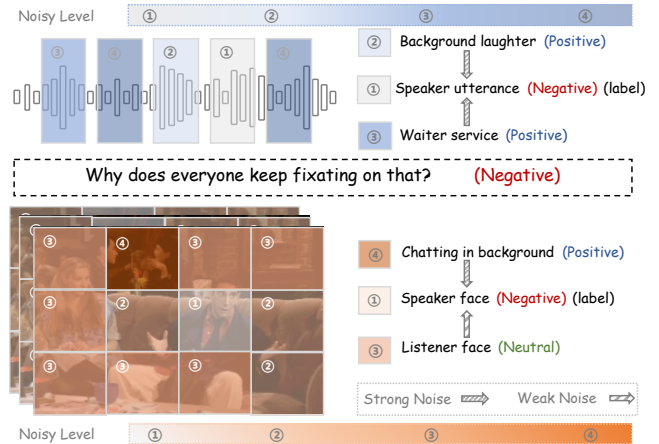


Figure 1: Distribution of noise. Lighter colors in the region mean more noise and less useful information.

modalities, for example, text, audio, and visual data (Han, Chen, and Poria 2021; Wang 2022; Mai, Zeng, and Hu 2022; Wu et al. 2024; Xie et al. 2024; Li and Liu 2025; Lin et al. 2022). However, due to irrelevant and misleading noise, the application of MSA systems in real-world scenarios remains challenging. It has been demonstrated that misleading noise information can seriously interfere with the model’s representation learning and further lead to performance degradation (Li and Li 2025; Liu 2024; Mao et al. 2023). To deal with multiple noise patterns, a straightforward simple solution is to train individual models from scratch for each type of noise (Yuan et al. 2021; Li et al. 2020). This strategy relies on prior knowledge of characteristic noise, which is typically unavailable in practical applications. An intuitive improvement is to design a unified model to adaptively perceive noise features (Zeng, Zhou, and Liu 2022b). However, there are significant differences among various types of modality-specific noise. For instance, noise in the visual modality is usually caused by non-target person interference, while noise in the audio modality mainly comes from the environmental background. Consequently, a model optimized for a specific type of feature noise may yield suboptimal performance when applied to other noise modalities. To address this limitation, researchers design different denois-

ing methods based on the characteristics of different noise for each noise pattern. (Yuan et al. 2023, 2024). Notably, the intensity and contribution of noise differ across regions within each modality. Therefore, those approaches that denoise the entire modality as a whole may suppress noise information at the cost of losing essential information.

As shown in Figure 1, different modalities contain noise that is inconsistent with the sentiment labels, and the intensity of this noise varies across different regions. Specifically, the visual modality contains visual noise that contradicts Ross’s emotional state, such as people’s smiles in the background, which constitute strong noise. While other parts of the background represent weak noise. Similarly, the audio contains segments of strong noise, such as laughter, that conflict with the sentiment label. The inconsistency of the noise distribution highlights the importance of fine-grained denoising that can distinguish between varying levels of noise intensity and selectively suppress noise information without losing essential information. Therefore, the challenge of this paper is how to perform fine-grained noise dynamic editing on different modalities, so as to remove noise information while retaining information that is beneficial to MSA.

To address these issues, we propose **MoLAN**, a unified **ModaLity**-aware noise **dynAmic editiNg** framework. To achieve dynamic fine-grained denoising, MoLAN employs a blocking strategy that divides each modality into different sub-blocks. In each block, the denoising strength is dynamically computed based on the noise level of the block. This approach allows the model to apply varying degrees of denoising across different blocks, thereby enhancing its ability of selective noise editing while preserving essential information in each modality. In addition, due to the heterogeneity between different modalities (Fan et al. 2024; Wei et al. 2023), we adopt different block strategies for different modalities. The visual modality uses two-dimensional blocks, while the audio modality uses one-dimensional blocks. Following previous works (Li and Li 2025; Zhang et al. 2023; Lin and Hu 2022), we choose text as the main modality to calculate the denoising strength. Additionally, MoLAN is a unified framework that can be flexibly integrated into different MSA methods to improve the upper limit of model performance. Based on the MoLAN, we propose **MoLAN⁺**, which uses denoised information to update the cross-attention between modalities and guide the model to focus on important information for MSA. MoLAN⁺ further introduces denoising-driven contrastive learning to encourage the model to generate higher quality features, improving the performance of MSA task. The key contributions of our work are as follows:

- To address the noise problem, we propose **MoLAN**, a unified **ModaLity**-aware noise **dynAmic editiNg** framework. MoLAN performs modality-aware blocking by dividing the modality features into multiple blocks. Each block is dynamically assigned a distinct denoising strength, enabling fine-grained noise editing. Additionally, MoLAN can be flexibly integrated into various MSA models.
- Based on the denoising framework, we further intro-

duce the noise suppression cross-attention mechanism and denoising-driven contrastive learning, and design an MSA method **MoLAN⁺**. MoLAN⁺ suppresses noise and guides the model to generate higher quality features.

- We conduct experiments on five models and four datasets to demonstrate the broad effectiveness of the MoLAN framework. Additionally, extensive evaluations on four benchmark multimodal datasets show that MoLAN⁺ achieves the state-of-the-art performance.

Related Work

Multimodal Sentiment Analysis (MSA)

MSA aims to enable machines to understand human emotions by leveraging multimodal signals. Early MSA research primarily employs methods such as TFN (Zadeh et al. 2017) and LMF (Liu and Shen 2018) to obtain multimodal fused representations through different feature extraction networks. As technology advances, researchers explore the use of Transformer encoder architectures (Vaswani et al. 2017; Tsai et al. 2019a) to achieve alignment between different modalities. Similarly, several studies based on cross-modal attention mechanisms (Goncalves and Busso 2022; Wu et al. 2024; Paraskevopoulos, Georgiou, and Potamianos 2022) provide insights into more effective strategies for aligning multimodal data. Moreover, knowledge is incorporated into the process of integrating multimodal information. KuDA (Feng et al. 2024) leverages affective knowledge to dynamically guide the model in selecting the dominant modality and adjusting the contribution of each modality, while the KEBR (Zhu et al. 2024) injects non-verbal information from videos into the semantic representations of text, thereby enhancing the multimodal representation of textual data. Although most works make progress in the alignment and integration of multimodal information, they ignore the impact of modality noise, thus limiting the performance of the model. Our work dynamically edits the noise in different modality information to improve the performance of MSA.

Multimodal Sentiment Analysis Denoising

Recently, noise in MSA has attracted the attention of researchers. The t-HNE (Li and Li 2025) removes noise from vision and audio through text guidance and attention mechanism. Meta-NA (Zeng, Zhou, and Liu 2022b) learning strategy uses meta-learning to simulate noise tasks and train the model to deal with noise data. JOSFD (Jiang et al. 2024) introduces fuzzy logic into the multimodal fusion and decision-making process to effectively model the subjective and objective ambiguity of emotions. In addition, missing modality is also regarded as a kind of noise in MSA, and thus receives extensive attention (Zeng, Liu, and Zhou 2022; Li et al. 2024). However, research on missing modality mainly focuses on modality completion (Zeng, Zhou, and Liu 2022a) or reducing the interference of missing modality (Shi et al. 2024), and pays insufficient attention to the problem of noise in the original modality. Although modal noise attracts attention, most methods are too coarse in denoising, treating each modality as an independent denoising

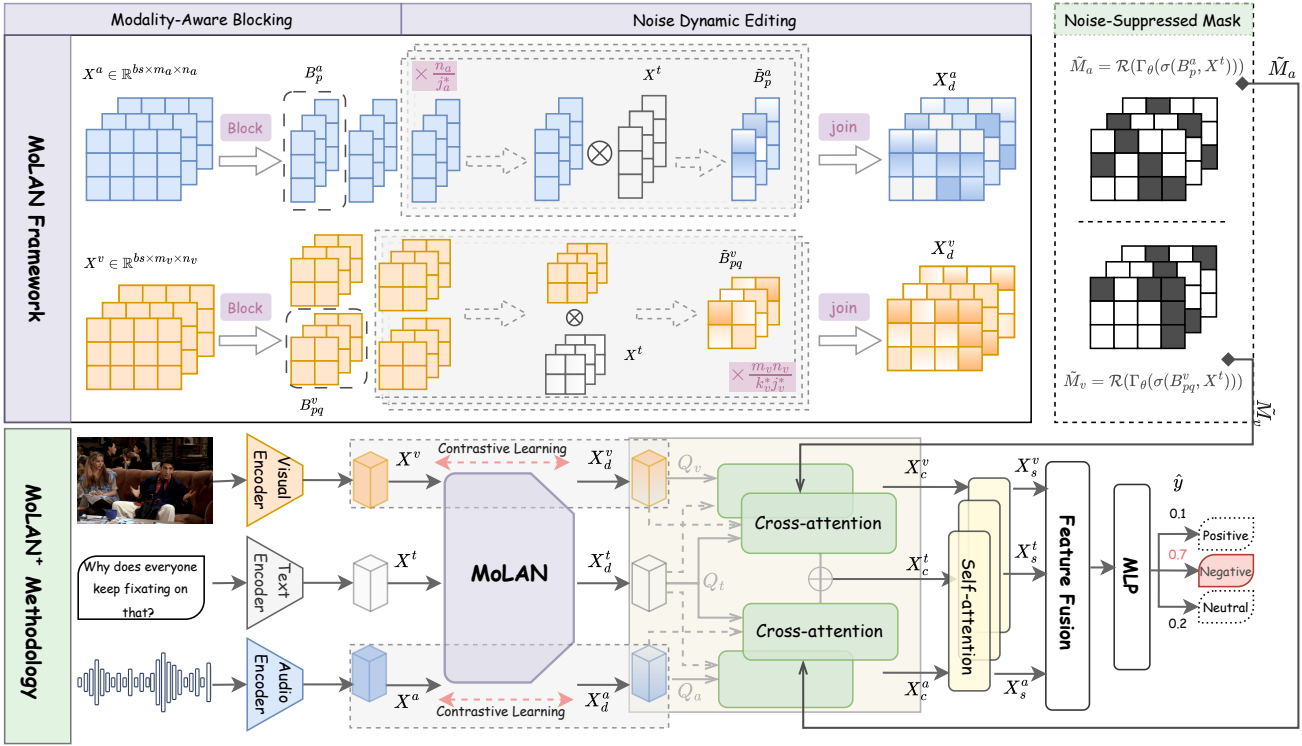


Figure 2: An illustration of our proposed MoLAN framework and MoLAN⁺ method. The purple box above represents the MoLAN framework, and the below represents the entire process of the framework-based MoLAN⁺ method. The MoLAN framework shown above provides a detailed description of the MoLAN block presented in MoLAN⁺ method.

unit. This approach may lose key information due to excessive denoising, or retain noise due to incomplete processing. In contrast, this study proposes a fine-grained modal noise dynamic editing strategy to effectively remove noise while retaining important information.

MoLAN Framework

As shown in the purple box in the upper part of Figure 2, the MoLAN framework consists of two components: modality-aware blocking and noise dynamic editing. The framework input is the encoder output of the MSA model.

Modality-Aware Blocking

Since the distribution of noise is uneven, we introduce a block-level mechanism to enable fine-grained control over the denoising range. Through blocking, the minimum unit of the denoising operation shifts from the entire modality feature to a feature block, thereby achieving more precise denoising. Considering the differences between modalities, visual information usually presents in regional forms, which is suitable for two-dimensional blocking. In contrast, audio information appears as continuous segments, so one-dimensional blocking is more effective. Feature representation of modalities as $X^f \in \mathbb{R}^{bs \times m_f \times n_f}$, $f \in t, a, v$.

$$P_{block} = \begin{cases} (k_v^*, j_v^*), & \text{if } f = v \\ (j_a^*), & \text{if } f = a \end{cases} \quad (1)$$

where P_{block} is the optimal blocking parameter, it represents the size of the block. bs is batch size. We use two-dimensional blocking as an example to illustrate the blocking process. (k_v^*, j_v^*) is calculated as:

$$(k_v^*, j_v^*) = \arg \min_{(k_v, j_v) \in \mathcal{D}_{m_v} \times \mathcal{D}_{n_v}} \left\| \frac{k_v}{\sqrt{m_v}} - 1 \right\|_2^2 + \left\| \frac{j_v}{\sqrt{n_v}} - 1 \right\|_2^2 \quad (2)$$

where \mathcal{D}_m and \mathcal{D}_n represent the sets of factors k_v and j_v of m_v and n_v , respectively. The $\| \cdot \|_2^2$ represents the square of the L2 norm. Using the factor closest to the square root as the basis for block division can achieve balanced segmentation: it can avoid information loss or noise residue caused by too large blocks, and semantic loss caused by too small blocks. The modality feature X^v is reshaped according to the block parameters, and each sub-block is defined as:

$$B_{pq}^v = X^v \left[(p-1)k_v^*, (q-1)j_v^* \right], \quad \forall p \in \left[1, \frac{m_v}{k_v^*} \right], q \in \left[1, \frac{n_v}{j_v^*} \right] \quad (3)$$

where $B_{pq}^v \in \mathbb{R}^{bs \times k_v^* \times j_v^*}$. p and q index the row and column positions of the sub-blocks. See the supplementary material for more detailed reasons for selecting factors for block partitioning based on square root.

Noise Dynamic Editing

We first dynamically compute the adaptive denoising strength of each sub-block B_{pq}^v and then edit its noise ac-

cordingly. The denoising strength is calculated as follows:

$$\sigma(B_{pq}^v, X^t) = \frac{\langle \Phi(B_{pq}^v), \Psi(X^t) \rangle}{\|\Phi(B_{pq}^v)\|_2 \cdot \|\Psi(X^t)\|_2} \quad (4)$$

where X^t is text vector. Φ and Ψ is a mapping function. σ is the denoising strength for the block B_{pq}^v . Based on this strength, we perform dynamic editing. The denoising operation for each sub-block B_{pq}^v can be represented as:

$$\tilde{B}_{pq}^v = \sigma(B_{pq}^v, X^t) \cdot B_{pq}^v \quad (5)$$

The denoised feature is obtained by recombining all blocks:

$$X_d^v = R(\{\tilde{B}_{pq}^v\}_{p=1, q=1}^{P, Q}) \quad (6)$$

where $X_d^v \in R^{bs \times m_v \times n_v}$. \mathcal{R} is the block reassembly operator. P, Q is total block numbers. $P = m_v/k_v^*$, $Q = n_v/j_v^*$.

MoLAN+ Methodology

As shown in Figure 2, we propose the MoLAN+ method built upon MoLAN framework. The MoLAN+ method consists of three components: the MoLAN framework, noise-suppressed cross attention, and denoise-driven contrastive learning. The detailed introduction of each module can be found in following subsections.

Problem Definition

In MSA task, the input signal consists of $text(t)$, $visual(v)$ and $audio(a)$ modalities. The feature representation of these modalities can be denoted as $X^f \in R^{bs \times m_f \times n_f}$, $f \in t, a, v$. The prediction is the sentiment score \hat{y} , which is a value.

To ensure a fair comparison, we use the same feature encoder as previous work (Tsai et al. 2019a; Wu et al. 2024; Sun and Tian 2025a). After encoding, we feed the modality features into the MoLAN to obtain the denoised features:

$$X_d^v, X_d^a = MoLAN(X^t, X^v, X^a) \quad (7)$$

Noise-Suppressed Cross Attention

In the green module below of Figure 2, to further enhance noise suppression, we update the attention mechanism based on the denoising strength calculation information. Take visual modality as an example:

$$M_{pq}^v = \Gamma_\theta(\sigma(B_{pq}^v, X^t)) \in \{0, 1\} \quad (8)$$

$$\Gamma_\theta(\sigma(B_{pq}^v, X^t)) = I(\sigma(B_{pq}^v, X^t) \geq \theta) \odot J_{pq} \quad (9)$$

where $I(\cdot)$ is the indicator function. J_{pq} is an all-ones matrix. $\theta \in [0, 1]$ is the fixed similarity threshold. We aggregate the sub-blocks together to construct the mask matrix.

$$\tilde{M}_v = \mathcal{R}(\{M_{pq}^v\}_{p=1, q=1}^{P, Q}) \quad (10)$$

where \mathcal{R} is the block reassembly operator that joins the sub-blocks according to their original positions. The mask matrix derived from the MoLAN is combined to calculate the cross-modality attention score to reduce the impact of noise.

$$X_c^{f_q} = \Omega_{\text{Inter-M}}(X_d^{f_q}, X_d^{f_{kv}}, \tilde{M}_{f_q}) \quad (11)$$

$$\Omega_{\text{Inter-M}}(X_d^{f_q}, X_d^{f_{kv}}, X_d^{f_{kv}}, \tilde{M}_{f_q}) = \frac{\exp_i[X_d^{f_q} X_d^{f_{kv}T} \cdot (\sqrt{d})^{-1} + \tilde{M}_{mq}]}{\sum \exp_j[X_d^{f_q} X_d^{f_{kv}T} \cdot (\sqrt{d})^{-1} + \tilde{M}_{mq}]} X_d^{f_{kv}} \quad (12)$$

where $f_q, f_{kv} \in \{t, a, v\}$. The text attention mask matrix is generated by the encoder. $X_c^{f_q}$ represents the feature after the attention mechanism.

Denoise-Driven Contrastive Learning

As shown in the light gray below of Figure 2, we introduce a noise-driven contrastive learning loss. We perform contrastive learning on the denoised features and their corresponding original features to encourage the model to learn more discriminative denoised representations. The contrastive learning loss function is as follows:

$$\begin{aligned} \mathcal{L}_{\text{contrast}} = & \\ & - E_{(X^v, X^a) \sim \rho} \log \left[\frac{\exp(\phi(X_d^v, X^v)/\tau)}{\sum_{j=1}^N \exp(\phi(X_d^v, X_j^v)/\tau)} \right] \\ & - E_{(X^v, X^a) \sim \rho} \log \left[\frac{\exp(\psi(X_d^a, X^a)/\tau)}{\sum_{j=1}^N \exp(\psi(X_d^a, X_j^a)/\tau)} \right] \end{aligned} \quad (13)$$

where ϕ and ψ denote similarity measurement functions, with cosine similarity adopted in this work. τ is a temperature parameter that controls the smoothness of the distribution. During training, this module guides the encoder to focus on distinguishing modal noise, thereby improving the overall denoising quality and the effectiveness of multi-modal fusion.

Sentiment Prediction

By introducing a cross-attention mechanism, information from different modalities is effectively interacted and integrated, enabling the initial fusion of multimodal features. Subsequently, the interacted representations are fed into a self-attention mechanism to further model the deep intra-modal dependencies. Finally, the information from different modalities is consolidated into a unified representation, which is used for the sentiment analysis task.

$$X_s^f = \text{SelfAttn}(X_c^f, \tilde{M}_f) \quad (14)$$

$$\hat{y} = \text{MLP}_{\theta_{\text{FC}}}(\mathcal{F}_{\text{fuse}}(\text{Cat}(X_s^t, X_s^a, X_s^v))) \quad (15)$$

where θ_{FC} denotes the parameters of the fully connected network. $\mathcal{F}_{\text{fuse}}$ denotes linear layer, and \hat{y} is the predicted sentiment value. The overall training of the MoLAN+ is performed by minimizing the following loss:

$$\mathcal{L} = \mathcal{L}_{\text{task}} + \mathcal{L}_{\text{contrast}}^v + \mathcal{L}_{\text{contrast}}^a \quad (16)$$

where $\mathcal{L}_{\text{task}}$ involves regression and classification tasks. For regression tasks, we adopt the L1 loss. For classification tasks, the standard cross-entropy loss is employed to optimize the model. The loss of the predicted value \hat{y} and the

Model	CMU-MOSI					CMU-MOSEI				
	Acc ₂	F1	Acc ₇	MAE ↓	Corr	Acc ₂	F1	Acc ₇	MAE ↓	Corr
MuT	75.93/77.94	75.68/77.69	35.78	94.94	65.91	77.69/79.19	77.99/79.60	48.65	62.99	65.33
+MoLAN	78.85/81.04	77.97/80.57	36.71	91.40	68.56	78.50/81.19	78.32/81.16	49.52	61.95	66.44
SPECTRA	84.12/86.33	83.96/86.04	47.12	79.41	75.69	83.11/85.34	82.16/85.71	51.37	58.49	74.19
+MoLAN	85.13/86.79	84.53/86.69	48.27	78.28	76.41	84.36/85.79	83.56/86.60	52.69	56.41	75.14
KuDA	84.00/85.92	83.78/86.06	46.54	71.10	78.35	82.95/86.14	82.61/86.24	51.54	53.35	76.71
+MoLAN	85.92/87.31	86.05/88.12	48.23	70.11	80.15	84.55/87.35	84.2/88.00	53.33	51.27	78.84
SFTTR	81.73/83.15	82.54/84.05	45.95	71.37	78.99	82.17/85.27	82.79/85.64	53.12	53.95	76.33
+MoLAN	83.65/85.62	84.04/86.25	47.17	68.94	80.15	83.11/86.24	83.54/86.63	54.29	51.97	78.36
MMML	86.91/88.92	86.92/88.97	49.71	58.20	87.05	86.43/87.96	86.45/87.76	53.39	52.24	81.39
+MoLAN	87.72/89.30	87.69/89.33	50.61	58.27	87.46	86.85/88.10	86.53/87.88	55.11	51.45	81.66

Table 1: The performance of the MoLAN framework on the MOSI and MOSEI. The baseline results in the experiment are obtained through replication. Two evaluation metrics, ACC and F1, are adopted, specifically $ACC_{2Has0} / ACC_{2Non0}$ and $F1_{Has0} / F1_{Non0}$. We perform significance testing on five experimental groups, with p-value of 5.33×10^{-5} , 1.43×10^{-6} , 4.87×10^{-10} , 2.68×10^{-6} , and 2.16×10^{-3} , all of which < 0.05 indicate significant differences.

ground truth y is:

$$\mathcal{L}_{\text{task}} = \begin{cases} \mathcal{L}_{\text{reg}} = \frac{1}{N} \sum_{i=1}^N |y_i - \hat{y}_i| & \text{(Regression)} \\ \mathcal{L}_{\text{cla}} = \frac{1}{N} \sum_{i=1}^N -y_i \log(\hat{y}_i) & \text{(Classification)} \end{cases} \quad (17)$$

where N is the number of the samples. The model is trained based on the overall loss function.

Experiments

Datasets and Evaluation Metrics

We conduct experiments on CMU-MOSI (Zadeh et al. 2016), CMU-MOSEI (Zadeh et al. 2018a), CH-SIMS (Yu et al. 2020), and IEMOCAP (Busso et al. 2008). For the CMU-MOSI and CMU-MOSEI datasets, we follow prior works (Wu et al. 2024; Jiang et al. 2024; Zhuang et al. 2024) to evaluate both regression and classification tasks. For regression, we report the **Mean Absolute Error (MAE)** and **Correlation coefficient (Corr)**. For classification, we calculate the **Acc₂** and **F1** scores for both the including zero sentiment scores as positive ($ACC_{2Has0} / F1_{Has0}$) and the ignoring zero sentiment scores ($ACC_{2Non0} / F1_{Non0}$). Additionally, we report **Acc₇**. For the CH-SIMS dataset, we adopt **Acc₂** and **F1** scores as evaluation metrics for the classification task. For the IEMOCAP dataset, we use **Weighted-F1** and **Macro-F1** scores to assess task performance.

Baselines and Implementation Detail

In the framework experiments, we select influential and reproducible multimodal sentiment analysis models as comparative baselines: **MuT** (Tsai et al. 2019a), **SPECTRA** (Yu et al. 2023), **KuDA** (Feng et al. 2024), **SFTTR** (Sun and Tian 2025b), **MMML** (Wu et al. 2024).

In the methodological experiments, in addition to the baseline models used in the framework experiments, we also compare a series of representative approaches for multimodal sentiment analysis: **TFN** (Zadeh et al. 2017), **LMF**

Model	CH-SIMS		IEMOCAP	
	ACC ₂	F1	Weighted-F1	Macro-F1
MuT	68.49	55.68	65.07	65.38
+MoLAN	69.24	58.37	66.35	66.37
SPECTRA	77.12	77.06	63.21	63.54
+MoLAN	78.05	78.00	64.33	64.36
KuDA	78.54	78.41	64.00	63.86
+MoLAN	80.23	80.12	65.27	64.92
SFTTR	79.22	79.20	64.05	61.54
+MoLAN	80.96	80.39	65.61	62.94
MMML	79.39	79.50	64.29	62.86
+MoLAN	81.36	81.14	67.35	66.53

Table 2: The performance of the MoLAN framework on the SIMS and IEMOCAP. We perform significance testing on five experimental groups, with p-value of 4.26×10^{-2} , 6.01×10^{-4} , 2.95×10^{-3} , 1.08×10^{-3} , and 1.19×10^{-2} , all of which < 0.05 indicate significant differences.

(Liu et al. 2018), **MFM** (Tsai et al. 2019b), **Self-MM** (Yu et al. 2021), **UniMSE** (Hu et al. 2022), **CHFV** (Guo et al. 2022), **ALMT** (Zhang et al. 2023), **EMT** (Sun et al. 2023), **GLoMo** (Zhuang et al. 2024), **JOSFD** (Jiang et al. 2024), **t-HNE** (Li and Li 2025). **t-HNE** is the **latest** MSA denoising method. **MMML** is the current **SOTA** MSA model.

All experiments are conducted using the PyTorch framework on a hardware setup with 8 RTX A6000 GPUs. For the framework experiments, we strictly follow the hyperparameter settings reported in the original papers to ensure fair and consistent comparisons.

Framework Overall Analysis

Framework effectiveness. We extensively validate the MoLAN framework using five different methods in four standard datasets, with detailed experimental results shown in Table 1 and Table 2. The results clearly demonstrate that after integrating our framework, the performance of models improves. This phenomenon shows that the MoLAN frame-

Model	CMU-MOSI					CMU-MOSEI				
	ACC ₂	F1	ACC ₇	MAE ↓	Corr	ACC ₂	F1	ACC ₇	MAE ↓	Corr
TFN	-/80.80	-/80.70	34.90	90.10	69.80	-/82.50	-/82.10	50.20	59.30	67.70
LMF	-/82.50	-/82.40	33.20	91.70	69.50	-/82.00	-/82.10	48.00	62.30	70.00
MFM	-/81.70	-/81.60	35.40	87.70	70.60	-/84.40	-/84.30	51.30	56.80	70.30
MuT \diamond	75.93/77.94	75.68/77.69	35.78	94.94	65.91	77.99/79.60	77.99/79.60	48.65	62.99	65.33
Self-MM	84.00/84.42	85.98/85.95	-	71.30	79.80	82.81/82.53	85.17/85.30	-	53.00	76.50
UniMSE	85.85/86.90	85.83/86.42	48.68	69.10	80.90	85.86/87.50	85.79/87.46	54.39	52.30	77.30
CHFN	84.30/86.40	84.20/86.20	48.60	68.90	80.90	83.70/86.20	83.90/86.10	54.30	52.50	77.80
SPECTRA \diamond	84.12/86.33	83.96/86.04	47.12	79.41	75.69	83.11/85.34	82.16/85.71	51.37	58.49	74.19
ALMT	84.55/86.43	84.57/86.47	49.42	68.30	80.50	84.78/86.79	85.19/86.86	54.28	52.60	77.90
EMT	83.30/85.00	83.20/85.00	47.40	70.50	79.80	83.40/86.00	83.70/86.00	54.50	52.70	77.40
GLoMo	84.10/86.70	83.90/86.60	48.30	71.80	78.20	83.70/86.50	84.00/86.40	55.00	53.90	77.10
MMML \diamond	86.91/88.92	86.92/88.97	49.71	58.20	87.05	86.43/87.96	86.45/87.76	53.39	52.24	81.39
JOSFD \dagger	-/89.80	-/89.70	52.10	57.90	87.40	-/87.90	-/87.90	51.80	51.50	79.70
t-HNE \dagger	85.02/87.03	84.98/87.01	47.04	68.00	81.00	85.20/87.14	85.32/87.59	54.05	52.00	78.90
MoLAN ⁺	88.02/89.94	87.96/89.90	52.30	57.00	87.72	87.79/88.29	87.46/88.21	56.86	49.09	82.02

Table 3: The performance of the MoLAN⁺ method on the MOSI and MOSEI. \diamond indicates our reproduced results, while the other results are reported from the original papers. \dagger indicates MSA denoising method. We perform significance testing on MMML and MoLAN⁺, with p-value of $7.52 \times 10^{-4} < 0.05$ indicates significant differences. The best results are in bold.

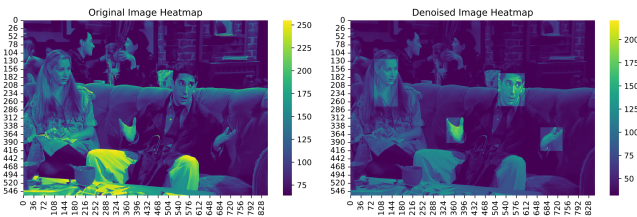


Figure 3: Pixel-level heatmap. Color intensity indicates the magnitude of the pixel value, with brighter areas representing stronger image information.

work suppresses noise while preserving essential information by performing fine-grained noise editing on modality information, thereby improving the performance upper limit of the model. Notably, even current SOTA method MMML benefits from performance enhancements upon applying our framework. These results further illustrate that existing methods inadequately address denoising.

Framework generalization. Furthermore, we observe that regardless of the specific model to which the framework is applied, the performance consistently exhibits a stable upward trend. This strongly validates the excellent generalization capability of our framework across various models and datasets. The performance of MoLAN on multiple experiments further demonstrates the generalization.

Effectiveness of Dynamic Strategy

The superior performance of the framework demonstrates the effectiveness of our proposed noise dynamic editing. Next, we illustrate the key role of noise dynamic editing from the perspectives of visualization. Figure 3 shows the heatmap comparison between the original image and the image processed by the MoLAN framework. It can be clearly

Model	CH-SIMS		IEMOCAP	
	ACC2	F1	Weighted-F1	Macro-F1
MuT \diamond	68.49	55.68	65.07	65.38
SPECTRA \diamond	77.12	77.06	63.21	63.54
KuDA \diamond	78.54	78.41	64.00	63.86
SFTTR \diamond	79.22	79.20	64.05	61.54
ALMT	81.19	81.57	-	-
MMML \diamond	79.39	79.50	64.29	62.86
MoLAN ⁺	82.24	81.63	68.79	67.69

Table 4: Performance of MoLAN⁺ on the SIMS and IEMOCAP. The significance testing on MMML and MoLAN⁺, with p-value ($0.01 < 0.05$) indicating significant differences.

observed that the energy distribution of the heatmap of the original image is uniform, and the emotional information (the target person’s face and hands) is not prominent enough due to the noise in the background area. After the noise dynamic editing of the MoLAN framework, the energy distribution of the heatmap on the right changes significantly. For the background noise area, the overall energy level is reduced, effectively suppressing the noise. In contrast, energy levels in areas such as the face remain high, forming clear highlights. This phenomenon intuitively illustrates that the MoLAN framework can dynamically control the area and intensity of noise editing, effectively removing noise while retaining essential information.

Methodological Experiments

We conduct experiments on the MoLAN⁺ method using four datasets. As shown in Table 3 and Table 4, MoLAN⁺ outperforms the existing baselines on four datasets and achieves SOTA performance. This indicates that the introduction of

Model	CMU-MOSI			CMU-MOSEI		
	ACC ₂	F1	Corr	ACC ₂	F1	Corr
MuT ⁺	81.04	80.57	68.56	81.19	81.16	66.44
w/o DE	78.25	78.20	66.49	79.29	79.93	65.47
w/o MB	78.65	78.43	66.97	79.82	79.73	65.61
MoLAN ⁺	89.94	89.90	87.72	88.29	88.21	82.02
w/o NC	89.69	89.68	87.59	88.16	87.96	81.85
w/o DC	89.74	89.71	87.64	88.20	88.01	81.88

Table 5: Ablation studies. MuT⁺ means MuT+MoLAN. DE indicates that dynamic editing. MB indicates that modality-aware blocking. NC means noise-suppressed cross attention. DC means denoise-driven contrastive learning.

the noise-suppression cross attention and noise-driven contrastive learning effectively helps the model capture more representative features, reducing the interference of noise on model performance.

Comparing the two MSA models based on denoising methods, JOSFD and t-HNE, the significance testing p-values are 0.01 and 4.85×10^{-5} , respectively, both less than 0.05. The MoLAN⁺ still has significant advantages. This shows that the method damages the model performance at the cost of losing essential information during the denoising process. However, MoLAN⁺ uses technologies such as noise dynamic editing to retain essential information for the MSA task while denoising, thus improving the task performance.

As shown in Figure 4, we conduct a case study comparing the original sota model MMML and the latest denoising model t-HNE. In the example on the left of the figure, we compare it with MMML. It can be seen that MMML pays equal attention to modality information in different regions/segments and does not eliminate the influence of noise. In the example on the right of the figure, we compare it with t-HNE. It can be seen that t-HNE uses a consistent denoising intensity in denoising, which leads to the loss of necessary information and causes incorrect sentiment analysis.

Ablation Study

As shown in the upper part of Table 5, we first conduct ablation experiments on two parts of MoLAN framework.

Effectiveness of noise dynamic editing. We apply a uniform denoising strength to the modality information. Experimental results (w/o DE) show that the model performance degrades after removing dynamic editing. This indicates that uniform denoising strength cannot handle the differences in noise levels between different regions. This method under-dennoises the high-noise regions and over-dennoises the low-noise regions, resulting in information loss.

Effectiveness of modality-aware blocking. In addition, we conduct an ablation study on the modality-aware blocking (w/o MB). We use uniform one-dimensional blocking to all modalities. The experimental results show that the model performance has degraded. This shows that the information distribution between different modalities is different, and only by adopting a targeted blocking strategy can the noise be located and processed more effectively.

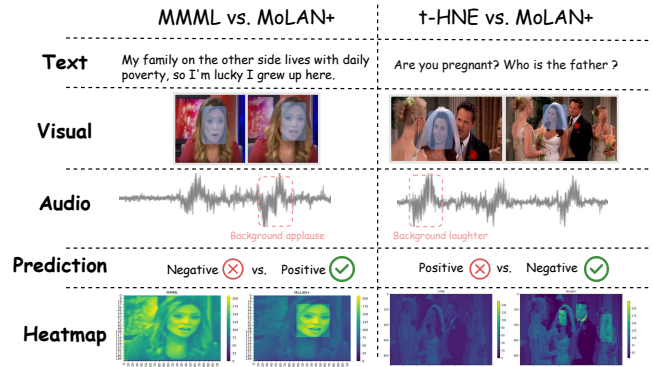


Figure 4: Case Study. Blue indicates the target person.

As shown in the lower part of Table 5, we perform ablation experiments of the two modules of MoLAN⁺.

Effectiveness of noise-suppressed cross attention. We remove the noise-suppressed cross attention (w/o NC). The results show a decline in model performance. This suggests that denoising information is crucial for the computation of the cross-attention mechanism. After removing the mask matrix, the model’s ability to perceive noise decreases, leading to an overall performance drop. Therefore, incorporating the mask matrix with denoising information can effectively guide the cross-attention computation.

Effectiveness of denoise-driven contrastive learning. We remove the denoise-driven contrastive learning (w/o DC). The decline of performance indicates that contrastive learning plays a key role in the encoding of modality information during optimization. After removing this component, the model cannot fully utilize the relationship between denoised modality information and initial information, leading to a reduction in its ability to suppress noise during the feature extraction process. Therefore, noise-driven contrastive learning promotes the encoding of modality information. More ablation experiments see supplementary material.

Conclusion

In this paper, we propose MoLAN, a unified modality-aware noise dynamic editing framework. MoLAN adopts a differentiated block strategy to divide different modalities into blocks. Subsequently, the adaptive denoising strength is dynamically allocated according to the noise level and semantic relevance of each block, thus achieving noise editing. As a unified framework, MoLAN can be flexibly integrated into different MSA methods to improve the performance of the original model. In addition, based on the framework, we propose an MSA method MoLAN⁺. MoLAN⁺ introduces a noise suppression cross-attention mechanism and denoising-driven contrastive learning to guide the model to focus on essential information. Experiments on five models and four datasets verify the broad effectiveness of the MoLAN. Extensive evaluation on four multimodal benchmark datasets demonstrates that MoLAN⁺ achieves state-of-the-art performance. In the future, we will further explore the application potential of MoLAN in other multimodal tasks.

References

- Busso, C.; Bulut, M.; Lee, C.-C.; Kazemzadeh, E. A.; Provost, E. M.; Kim, S.; Chang, J. N.; Lee, S.; and Narayanan, S. S. 2008. IEMOCAP: interactive emotional dyadic motion capture database. *Language Resources and Evaluation*, 42: 335–359.
- Das, R.; and Singh, T. D. 2023. Multimodal sentiment analysis: a survey of methods, trends, and challenges. *ACM Computing Surveys*, 55(13s): 1–38.
- Fan, C.; Zhu, K.; Tao, J.; Yi, G.; Xue, J.; and Lv, Z. 2024. Multi-level contrastive learning: Hierarchical alleviation of heterogeneity in multimodal sentiment analysis. *IEEE Transactions on Affective Computing*.
- Feng, X.; Lin, Y.; He, L.; Li, Y.; Chang, L.; and Zhou, Y. 2024. Knowledge-Guided Dynamic Modality Attention Fusion Framework for Multimodal Sentiment Analysis. In *Findings of the Association for Computational Linguistics: EMNLP 2024*, 14755–14766.
- Goncalves, L.; and Busso, C. 2022. Robust audiovisual emotion recognition: Aligning modalities, capturing temporal information, and handling missing features. *IEEE Transactions on Affective Computing*, 13(4): 2156–2170.
- Guo, J.; Tang, J.; Dai, W.; Ding, Y.; and Kong, W. 2022. Dynamically Adjust Word Representations Using Unaligned Multimodal Information. In *Proceedings of the 30th ACM International Conference on Multimedia*, MM '22, 3394–3402. New York, NY, USA: Association for Computing Machinery. ISBN 9781450392037.
- Han, W.; Chen, H.; and Poria, S. 2021. Improving Multimodal Fusion with Hierarchical Mutual Information Maximization for Multimodal Sentiment Analysis. In *Proceedings of the 2021 Conference on Empirical Methods in Natural Language Processing*, 9180–9192.
- Hu, G.; Lin, T.-E.; Zhao, Y.; Lu, G.; Wu, Y.; and Li, Y. 2022. UniMSE: Towards Unified Multimodal Sentiment Analysis and Emotion Recognition. In *Proceedings of the 2022 Conference on Empirical Methods in Natural Language Processing*, 7837–7851. Abu Dhabi, United Arab Emirates: Association for Computational Linguistics.
- Jiang, X.; Xu, X.; Lu, H.; He, L.; and Shen, H. T. 2024. Joint objective and subjective fuzziness denoising for multimodal sentiment analysis. *IEEE Transactions on Fuzzy Systems*.
- Li, B.; Li, C.; Duan, F.; Zheng, N.; and Zhao, Q. 2020. TPFN: Applying outer product along time to multimodal sentiment analysis fusion on incomplete data. In *European Conference on Computer Vision*, 431–447. Springer.
- Li, M.; Yang, D.; Lei, Y.; Wang, S.; Wang, S.; Su, L.; Yang, K.; Wang, Y.; Sun, M.; and Zhang, L. 2024. A unified self-distillation framework for multimodal sentiment analysis with uncertain missing modalities. In *Proceedings of the AAAI conference on artificial intelligence*, volume 38, 10074–10082.
- Li, T.; and Liu, D. 2025. MPID: A Modality-Preserving and Interaction-Driven Fusion Network for Multimodal Sentiment Analysis. In *Proceedings of the 31st International Conference on Computational Linguistics*, 4313–4322.
- Li, Z.; and Li, L. 2025. t-HNE: A Text-guided Hierarchical Noise Eliminator for Multimodal Sentiment Analysis. In *Proceedings of the 31st International Conference on Computational Linguistics*, 2834–2844.
- Lin, R.; and Hu, H. 2022. Multimodal Contrastive Learning via Uni-Modal Coding and Cross-Modal Prediction for Multimodal Sentiment Analysis. In *Findings of the Association for Computational Linguistics: EMNLP 2022*, 511–523.
- Lin, Z.; Liang, B.; Long, Y.; Dang, Y.; Yang, M.; Zhang, M.; and Xu, R. 2022. Modeling intra-and inter-modal relations: Hierarchical graph contrastive learning for multimodal sentiment analysis. In *Proceedings of the 29th international conference on computational linguistics*, volume 29, 7124–7135. Association for Computational Linguistics.
- Liu, Y. e. a. 2024. Noise-resistant multimodal transformer for emotion recognition. *International Journal of Computer Vision*, 1–21.
- Liu, Z.; and Shen, Y. 2018. Efficient Low-rank Multimodal Fusion with Modality-Specific Factors. In *Proceedings of the 56th Annual Meeting of the Association for Computational Linguistics (Long Papers)*.
- Liu, Z.; Shen, Y.; Lakshminarasimhan, V. B.; Liang, P. P.; Bagher Zadeh, A.; and Morency, L.-P. 2018. Efficient Low-rank Multimodal Fusion With Modality-Specific Factors. In Gurevych, I.; and Miyao, Y., eds., *Proceedings of the 56th Annual Meeting of the Association for Computational Linguistics (Volume 1: Long Papers)*, 2247–2256. Melbourne, Australia: Association for Computational Linguistics.
- Mai, S.; Zeng, Y.; and Hu, H. 2022. Multimodal information bottleneck: Learning minimal sufficient unimodal and multimodal representations. *IEEE Transactions on Multimedia*, 25: 4121–4134.
- Mao, H.; Zhang, B.; Xu, H.; Yuan, Z.; and Liu, Y. 2023. Robust-MSA: Understanding the impact of modality noise on multimodal sentiment analysis. In *Proceedings of the AAAI Conference on Artificial Intelligence*, volume 37, 16458–16460.
- Morency, L.-P.; Mihalcea, R.; and Doshi, P. 2011. Towards multimodal sentiment analysis: Harvesting opinions from the web. In *Proceedings of the 13th international conference on multimodal interfaces*, 169–176.
- Pantic, M.; and Rothkrantz, L. J. 2003. Toward an affect-sensitive multimodal human-computer interaction. *Proceedings of the IEEE*, 91(9): 1370–1390.
- Paraskevopoulos, G.; Georgiou, E.; and Potamianos, A. 2022. Mmlatch: Bottom-up top-down fusion for multimodal sentiment analysis. In *ICASSP 2022*, 4573–4577. IEEE.
- Shi, L.; Xu, F.; Wang, R.; Wei, Y.; Wang, G.; Wang, B.; and Liu, P. 2024. Information Aggregate and Sentiment Enhance Network to Handle Missing Modalities for Multimodal Sentiment Analysis. In *2024 ICME*, 1–6. IEEE.
- Sun, K.; and Tian, M. 2025a. Sequential fusion of text-close and text-far representations for multimodal sentiment analysis. In *Proceedings of the 31st international conference on computational linguistics*, 40–49.

- Sun, K.; and Tian, M. 2025b. Sequential Fusion of Text-close and Text-far Representations for Multimodal Sentiment Analysis. In Rambow, O.; Wanner, L.; Apidianaki, M.; Al-Khalifa, H.; Eugenio, B. D.; and Schockaert, S., eds., *Proceedings of the 31st International Conference on Computational Linguistics*, 40–49. Abu Dhabi, UAE: Association for Computational Linguistics.
- Sun, L.; Lian, Z.; Liu, B.; and Tao, J. 2023. Efficient multimodal transformer with dual-level feature restoration for robust multimodal sentiment analysis. *IEEE Transactions on Affective Computing*, 15(1): 309–325.
- Tsai, Y.-H. H.; Bai, S.; Liang, P. P.; Kolter, J. Z.; Morency, L.-P.; and Salakhutdinov, R. 2019a. Multimodal transformer for unaligned multimodal language sequences. In *Proceedings of the conference. Association for computational linguistics. Meeting*, volume 2019, 6558.
- Tsai, Y.-H. H.; Liang, P. P.; Zadeh, A.; Morency, L.-P.; and Salakhutdinov, R. 2019b. Learning Factorized Multimodal Representations. In *ICLR*.
- Vaswani, A.; Shazeer, N.; Parmar, N.; Uszkoreit, J.; Jones, L.; Gomez, A. N.; Kaiser, Ł.; and Polosukhin, I. 2017. Attention is all you need. *Advances in neural information processing systems*, 30.
- Wang, D. e. a. 2022. Cross-modal enhancement network for multimodal sentiment analysis. *IEEE Transactions on Multimedia*, 25: 4909–4921.
- Wei, Y.; Yuan, S.; Yang, R.; Shen, L.; Li, Z.; Wang, L.; and Chen, M. 2023. Tackling modality heterogeneity with multi-view calibration network for multimodal sentiment detection. In *Proceedings of the 61st Annual Meeting of the Association for Computational Linguistics (Volume 1: Long Papers)*, 5240–5252.
- Wu, Z.; Gong, Z.; Koo, J.; and Hirschberg, J. 2024. Multimodal Multi-loss Fusion Network for Sentiment Analysis. In *Proceedings of the 2024 NAACL*, 3588–3602.
- Xie, Y.; Zhu, Z.; Lu, X.; Huang, Z.; and Xiong, H. 2024. InfoEnh: Towards Multimodal Sentiment Analysis via Information Bottleneck Filter and Optimal Transport Alignment. In *Proceedings of the LREC-COLING 2024*, 9073–9083.
- Yu, T.; Gao, H.; Lin, T.-E.; Yang, M.; Wu, Y.; Ma, W.; Wang, C.; Huang, F.; and Li, Y. 2023. Speech-Text Pre-training for Spoken Dialog Understanding with Explicit Cross-Modal Alignment. In Rogers, A.; Boyd-Graber, J.; and Okazaki, N., eds., *Proceedings of the 61st ACL*, 7900–7913. Toronto, Canada: Association for Computational Linguistics.
- Yu, W.; Xu, H.; Meng, F.; Zhu, Y.; Ma, Y.; Wu, J.; Zou, J.; and Yang, K. 2020. CH-SIMS: A Chinese Multimodal Sentiment Analysis Dataset with Fine-grained Annotation of Modality. In *Annual Meeting of the Association for Computational Linguistics*.
- Yu, W.; Xu, H.; Yuan, Z.; and Wu, J. 2021. Learning Modality-Specific Representations with Self-Supervised Multi-Task Learning for Multimodal Sentiment Analysis. *Proceedings of the AAAI Conference on Artificial Intelligence*, 35(12): 10790–10797.
- Yuan, Z.; Li, W.; Xu, H.; and Yu, W. 2021. Transformer-based feature reconstruction network for robust multimodal sentiment analysis. In *Proceedings of the 29th ACM MM*, 4400–4407.
- Yuan, Z.; Liu, Y.; Xu, H.; and Gao, K. 2023. Noise imitation based adversarial training for robust multimodal sentiment analysis. *IEEE Transactions on Multimedia*.
- Yuan, Z.; Zhang, B.; Xu, H.; and Gao, K. 2024. Meta Noise Adaption Framework for Multimodal Sentiment Analysis With Feature Noise. *IEEE Transactions on Multimedia*, 26: 7265–7277.
- Zadeh, A.; Chen, M.; Poria, S.; Cambria, E.; and Morency, L.-P. 2017. Tensor Fusion Network for Multimodal Sentiment Analysis. In Palmer, M.; Hwa, R.; and Riedel, S., eds., *Proceedings of the 2017 Conference on Empirical Methods in Natural Language Processing*, 1103–1114. Copenhagen, Denmark: Association for Computational Linguistics.
- Zadeh, A.; Liang, P. P.; Poria, S.; Cambria, E.; and Morency, L.-P. 2018a. Multimodal Language Analysis in the Wild: CMU-MOSEI Dataset and Interpretable Dynamic Fusion Graph. In *Annual Meeting of the Association for Computational Linguistics*.
- Zadeh, A.; Liang, P. P.; Poria, S.; Vij, P.; Cambria, E.; and Morency, L.-P. 2018b. Multi-attention recurrent network for human communication comprehension. In *Proceedings of the AAAI conference on artificial intelligence*, volume 32.
- Zadeh, A.; Zellers, R.; Pincus, E.; and Morency, L.-P. 2016. MOSI: Multimodal Corpus of Sentiment Intensity and Subjectivity Analysis in Online Opinion Videos. *ArXiv*, abs/1606.06259.
- Zeng, J.; Liu, T.; and Zhou, J. 2022. Tag-assisted multimodal sentiment analysis under uncertain missing modalities. In *Proceedings of the 45th ACM SIGIR*, 1545–1554.
- Zeng, J.; Zhou, J.; and Liu, T. 2022a. Mitigating inconsistencies in multimodal sentiment analysis under uncertain missing modalities. In *Proceedings of the 2022 EMNLP*.
- Zeng, J.; Zhou, J.; and Liu, T. 2022b. Robust multimodal sentiment analysis via tag encoding of uncertain missing modalities. *IEEE Transactions on Multimedia*.
- Zhang, H.; Wang, Y.; Yin, G.; Liu, K.; Liu, Y.; and Yu, T. 2023. Learning Language-guided Adaptive Hyper-modality Representation for Multimodal Sentiment Analysis. In *Proceedings of the 2023 Conference on Empirical Methods in Natural Language Processing*, 756–767. Association for Computational Linguistics.
- Zhou, D.; Luo, J.; Silenzio, V.; Zhou, Y.; Hu, J.; Currier, G.; and Kautz, H. 2015. Tackling mental health by integrating unobtrusive multimodal sensing. In *Proceedings of the AAAI conference on artificial intelligence*, volume 29.
- Zhu, A.; Hu, M.; Wang, X.; Yang, J.; Tang, Y.; and Ren, F. 2024. KEBR: Knowledge Enhanced Self-Supervised Balanced Representation for Multimodal Sentiment Analysis. In *Proceedings of the 32nd ACM MM*, 5732–5741.
- Zhuang, Y.; Zhang, Y.; Hu, Z.; Zhang, X.; Deng, J.; and Ren, F. 2024. GLoMo: Global-Local Modal Fusion for Multimodal Sentiment Analysis. In *Proceedings of the 32nd ACM MM*, 1800–1809.

Pilot Study

The initial modality feature embedding, as the initial information after encoding, serves as the sole foundation for sentiment analysis by the model. However, existing research generally neglects the denoising of the encoded information from each modality and fails to thoroughly explore the impact of noise in the initial feature embedding. Noise within the initial features may interfere with the sentiment analysis outcomes. Enhancing the quality of initial features through effective denoising techniques holds promise for further improving the model’s performance. Therefore, we design and conduct a series of experiments to systematically analyze the noise present in the initial features.

Inspection Method

To investigate the impact of noise in initial multimodal feature information, we design a random masking strategy. Specifically, according to a predefined masking ratio, we randomly select elements within the feature embedding for masking.

$$M_{ij} = \begin{cases} 0, & \text{if } R_{ij} < p \\ 1, & \text{otherwise} \end{cases} \quad R_{ij} \sim \mathcal{U}(0, 1) \quad (18)$$

$$\tilde{\mathbf{F}} = \mathbf{F} \odot \mathbf{M} \quad (19)$$

where, \mathbf{f} denote the feature embedding matrix, and \mathbf{M} the corresponding mask matrix. Each element R_{ij} is a random number sampled from a uniform distribution over the interval $[0, 1]$. The masking ratio is defined by $p \in [0, 1]$.

If the initial feature information contains little noise, an intuitive inference is that the model performance will degrade as the masking ratio increases. Therefore, we gradually increase the masking ratio and observe the trend in model performance, thereby indirectly reflecting the level of potential noise in the initial multimodal features.

Ratio	MulT		MMML	
	CMU-MOSI	CMU-MOSEI	CMU-MOSI	CMU-MOSEI
10%	77.89	79.36	88.56	88.03
20%	79.42 ↑	79.27 ↓	88.63 ↑	86.96 ↓
30%	77.49 ↓	79.44 ↑	89.02 ↑	87.89 ↑
40%	79.57 ↑	80.10 ↑	88.63 ↓	87.84 ↓

Table 6: Multimodal Noise. ↓ indicates a performance drop compared to the previous row, while ↑ indicates an improvement. The metric used is ACC_2 .

Multimodal Noise

We first conduct a holistic modality masking experiment, in which we apply uniform masking to all modalities except for text. The models involved include widely used MulT models (Tsai et al. 2019a) as well as the latest SOTA models MMML (Wu et al. 2024). For visual features and audio features, we apply random masking at the same ratio. As shown in Table 6, the results indicate that as the masking ratio increases, model performance improves. This phenomenon suggests that the removed information may contain more noise than useful content, allowing the model to

perform better after eliminating these redundant features. These results further confirm that a large amount of noise exists in the initial modality features, and demonstrate that effective denoising strategies are likely to improve model performance.

Unimodal Noise

To further investigate the impact of noise within different modalities, we apply masking to each individual modality separately. Using the MulT model as the base framework, we impose varying levels of masking on the text, audio, and visual modalities. We observe how model performance changes as the degree of masking increases for each single modality. This allows us to analyze the relative level of noise in the initial features of each modality and its effect on sentiment analysis.

As shown in Table 7, the audio and visual modalities exhibit performance trends that differ from those of the text modality. As the masking ratio increases, the performance of the audio and visual modalities shows fluctuating improvements. However, performance consistently declines in the text modality. This observation suggests that the initial text modality features are higher quality, containing less noise. Therefore, the text modality can serve as a reference standard. Moreover, the performance improvements in the audio and visual modalities are triggered at different masking ratios, further validating the different distribution of noise across modalities. The performance under single modality masking surpasses that of simultaneously masking two modalities, indicating that applying a uniform masking strategy across all modalities leads to the loss of non-noise information. Therefore, differentiated denoising strategies should be adopted for different modalities.

Ratio	CMU-MOSI			CMU-MOSEI		
	Text	Visual	Audio	Text	Visual	Audio
10%	75.16	79.07	79.57	79.95	79.39	79.03
20%	71.91 ↓	80.16 ↑	77.77 ↓	75.06 ↓	79.42 ↑	79.13 ↑
30%	70.09 ↓	80.06 ↓	78.92 ↑	73.62 ↓	79.11 ↓	79.17 ↑
40%	66.83 ↓	79.41 ↓	78.43 ↓	73.46 ↓	78.78 ↓	77.98 ↓

Table 7: Unimodal Noise. Text, visual, and audio represent the modality being masked, while the other modality features remain unchanged.

Block Strategy Selection

Using square roots as the basis for block division can achieve relatively average division. This can avoid uneven noise distribution caused by too large a block size, which in turn causes excessive deletion of effective information or incomplete noise removal. It can also avoid the problem of incomplete semantics caused by too small a block size. As shown in Table 8, we design comparative experiments with various block sizes for visual and audio.

Experimental results show that in visual and audio information processing, too large or too small block size will lead to lower ACC values, while factors close to the square root as block size can fully capture effective information and

maintain information integrity. Overall, the square root as a block division basis has shown good results in both visual and audio modality, avoiding potential problems caused by too large or too small block size.

Block	Visual(50,2)	Visual(25,4)	Visual(20,4)	Visual(10,5)	Visual(5,10)
ACC	80.39	81.04	80.95	78.84	78.13
Block	Audio(3)	Audio(5)	Audio(15)	Audio(75)	Audio(125)
ACC	79.01	79.32	81.04	80.55	79.41

Table 8: Block Sizes Experiments. Take MulT+MoLAN on the CMU-MOSI dataset as an example. The audio feature dimension is [128, 375, 20], and the visual feature dimension is [128, 500, 20]. The number after audio indicates the one-dimensional block size (j), and the number after video indicates the two-dimensional block size (k, j).

Implementation Detail

All experiments are conducted using the PyTorch framework on a hardware setup with 8 RTX A6000 GPUs. For the framework experiments, we strictly follow the hyperparameter settings reported in the original papers to ensure fair and consistent comparisons. In the methodological experiments, all models are trained using the AdamW optimizer. Specifically, the learning rate is set to 5e-6 for the MOSI and MOSEI datasets, 1e-5 for the CH-SIMS dataset, and 2e-8 for the IEMOCAP dataset. To ensure the stability of the experimental results, we fix the random seed to 1 and run each experiment five times independently, reporting the average result.

More Ablation Experiments

MoLAN Framework

As shown in Table 9, we conduct ablation experiments on different parts of the MoLAN framework, including: (1) Using denoising methods only on video or only on audio modality. (2) Using 1D blocks for both video and audio. (3) Using 2D blocks for both video and audio. (4) Using 1D blocks for video and 2D blocks for audio.

Experimental results show that simultaneous block processing of visual and audio information can effectively filter out noise interference in each modality, thereby obtaining a more robust and discriminative feature representation. In further comparative experiments, we use multiple block dimensions. When the visual features are divided into two dimensions and the audio features are divided into one dimension, the model performance is optimal. This is highly consistent with the inherent structural characteristics of the two types of modalities. On the contrary, if the visual or audio information is divided in a block manner that does not match its information characteristics, it will lead to incomplete information after segmentation and loss of local features, which will lead to performance degradation. It can be seen that our block strategy improves denoising effects.

Denoise-Driven Contrastive Learning

To further verify the effectiveness of denoising-driven contrastive learning (DC) in modality denoising, we use two

Model	CMU-MOSI			CMU-MOSEI		
	ACC ₂	F1	Corr	ACC ₂	F1	Corr
MulT	77.94	77.69	65.91	79.19	79.60	65.33
MulT+MoLAN	81.04	80.57	68.56	81.19	81.16	66.44
w/o MoLAN(visual)	78.91	78.56	67.19	80.32	80.25	65.98
w/o MoLAN(audio)	79.15	78.95	67.95	80.65	80.76	66.10
Visual(1D), Audio(1D)	78.65	78.43	66.97	79.82	79.73	65.61
Visual(2D), Audio(2D)	79.48	79.68	68.19	80.20	80.59	66.04
Visual(1D), Audio(2D)	78.17	78.02	66.57	79.41	79.69	65.63

Table 9: MoLAN Framework Experiments. Take MulT as an example. 1D, 2D denote one-dimensional blocking and two-dimensional blocking, respectively.

metrics in the field of contrastive learning: alignment and uniformity. Alignment measures the average distance of the same positive sample pair in the embedding space. The smaller the value, the more closely the sample features are clustered. Uniformity reflects the degree of dispersion of all samples on the unit hypersphere. The lower the value, the greater the distance between negative sample pairs, and the noise is easier to distinguish.

Model	CMU-MOSI		CMU-MOSEI	
	Alignment ↓	Uniformity ↓	Alignment ↓	Uniformity ↓
w/o DC	0.9962	-0.5043	0.9993	-0.2674
with DC	0.9359	-2.2770	0.0198	-1.0030

Table 10: Ablation studies of Denoise-Driven Contrastive Learning.

As shown in Table 10, DC can enhance modality discrimination. After introducing DC, the alignment of positive sample pairs is further reduced, indicating that homologous samples are more closely clustered in the feature space. At the same time, the uniformity of negative sample pairs is significantly improved, indicating that the model’s ability to distinguish noisy samples has been greatly improved. This shows that DC plays a key role in the denoising process, enabling the model to learn denoising feature representations more efficiently, thereby improving the performance of MSA task.